Electrochemical Materials and Technologies

ARTICLE

Electrochemical Materials and Technologies

eISSN: 2949-0561

Cite this: Electrochem. Mater. Technol. 3 (2024) 20243030

Investigation of Raman spectra and ionic conductivity of composites based on $NaClO_4$ and $KClO_4$ salts obtained by mechanoactivation

Zaur Kubataev [a]*, Malik Gafurov [a], Kamil Rabadanov [a], Magomed Akhmedov [a], Akhmed Amirov [a]

Received: 27 November 2023
Accepted: 6 March 2024
Published online: 18 March 2024

DOI: 10.15826/elmattech.2024.3.030

The work is aimed at studying the effect of mechanical activation on the structure and electrical conductivity of the $NaClO_4$ – and $KClO_4$ – based composites. Based on the result of the analysis of the DSC curves of the $(1-x)\,NaClO_4 - x\,Al_2O_3$ and $(1-x)\,KClO_4 - x\,Al_2O_3$ composites measured while heating and cooling the samples, it was established that the enthalpy of phase transitions in them decreased with an increase in the concentration of the nanosized dopant. A complication of all active vibrational contours corresponding to internal vibrations of the molecular anion in the composites with increasing Al_2O_3 concentration and a shift of the band of the fully symmetric stretching vibration $\nu_1(A)$ to a low-frequency region was revealed by Raman spectroscopy. Based on electrochemical impedance spectroscopy data, it was determined that for the $0.4NaClO_4 - 0.6Al_2O_3$ system subjected to mechanoactivation, the values of specific ionic conductivity increased by two orders of magnitude as compared to that of pure $NaClO_4$, while for the $0.4KClO_4 - 0.6Al_2O_3$ system, the values of specific ionic conductivity increased by three orders of magnitude as compared to the initial salt at $T = 320$ °C.

keywords: composite, mechanical activation, Raman spectroscopy, aluminum oxide, activation energy, electrical conductivity

1. Introduction

In recent decades, electrochemical secondary batteries have received much attention as an efficient energy storage and conversion technology for integrating renewable resources [1, 2]. Lithium-ion batteries (LIBs) are very popular among them, and due to their high energy density, high output energy and long cycle operation, they have found wide application in modern life, for example, in portable electronics and electric vehicles [3, 4]. However, low Li salt reserves and increasing costs with the growth of demand have become an important problem. Therefore, there is a need to develop alternative energy storage systems to replace LIBs in the future and sodium (Na) batteries are considered as one of the most promising candidates due to high Na reserves, low cost, and comparative characteristics with LIBs [5, 6]. Yet, traditional Na batteries based on an organic liquid electrolyte still have safety problems such as liquid leakage, poor thermal stability, flammability, and explosion hazard, which are similar to those of LIBs based on a liquid electrolyte [7, 8]. A solid electrolyte has high thermal stability, low flammability, no leakage and volatilization, no fire and explosion risks as compared to an organic liquid electrolyte, which are favorable features for the development of all-solid-state Na batteries with high safety and stability. The search for composite electrolytes with high ionic conductivity is an important direction in solid state ionics [9, 10]. Composite solid electrolytes based on alkali metal salts and oxide powders are not always characterized by high values of specific ionic conductivity [11, 12].

The most popular method for producing salt-oxide composite electrolytes is the ceramic technique [13]. This

a: Analytical Center for Collective Use, Institute of Physics, Dagestan Federal Research Center, Russian Academy of Sciences, Makhachkala 367015, Russian Federation

* Corresponding author: kzu-05@ya.ru

technique involves impregnating the filler in the molten salt (salt system). The disadvantage of the ceramic technique is a uniform distribution of the filler particles in the molten salt due to their precipitation in the liquid phase. Thus, the ceramic technique rarely allows obtaining a single-phase composite with both a mesoporous structure and a relatively uniform distribution of filler particles in the composite salt subsystem [14, 15]. In addition, possible thermal decomposition of the salt upon melting during ceramic sintering should be taken into account.

Another method that ensures a relatively uniform distribution of elements in the composite, a reduction in particle size, the formation of a mesoporous structure and the production of a single-phase material is mechanical activation (MA) [16, 17].

Based on the above, in this work, we studied the effect of mechanical activation on the structure and electrical conductivity of the (1–x) $NaClO_4$ – x Al_2O_3 and (1–x) $KClO_4$ – x Al_2O_3 composites by differential scanning calorimetry (DSC), impedance spectroscopy, and Raman spectroscopy (RS).

2. Experimental

The (1–x) $NaClO_4$ – x Al_2O_3 and (1–x) $KClO_4$ – x Al_2O_3 composites were prepared using potassium and sodium perchlorate (analytical grade, Ecros) and nanocrystalline aluminum oxide γ–Al_2O_3 (Sigma Aldrich) with a specific surface area of 200 m^2/g and a particle size of ~ 15 nm.

2.1. Sample preparation procedure

The whole procedure of the preparation of the samples under study was carried out in a dry glove box in an inert atmosphere of high-purity argon (99.9999 wt. %). The initial $NaClO_4$ and $KClO_4$ salts and aluminum oxide were dehydrated for 2 days by heating at a temperature of 220 °C and pumping in a vacuum under a residual pressure of 10^{-3} Pa, and then placed in a vacuum glove box (Plas-Labs, USA). The accurately weighed $NaClO_4$ and $KClO_4$ salts and γ–Al_2O_3 weighed using analytical balances (Ohaus, Switzerland) were mixed and placed in a zirconium beaker (d = 53 mm, h = 55 mm) with zirconium balls (d = 5.8 and 8.2 mm). Mechanical activation (MA) was carried out using a laboratory ball mill ML-1 (VNIR, Russia). The MA time in vibration mode was 120 minutes.

2.2. Research methods

Studies by differential scanning calorimetry (DSC) were carried out using a Jupiter simultaneous thermal analyzer STA 449 F3 (NETZSCH, Germany) in the range from room temperature (20 °C) to the prescribed temperature at a heating rate of 10 °C/min in an argon atmosphere in platinum crucibles. The weight of the samples was about 8 mg. The resolution of the balance was 1 μg. Temperature and sensitivity calibrations were carried out using standard substances (Biphenyl, In, $RbNO_3$, KNO_3, $KClO_4$, Ag_2SO_4). Phase transition temperatures were determined according to the beginning of the peak. The temperature accuracy was ± 1.5 °C, the enthalpy accuracy was ± 3 %. Data processing and peak integration were conducted using the embedded application programs of the NETZSCH Company.

Electrochemical impedance was studied using an E7-20 RLC meter (MNIPI, Belarus) within the temperature range of 80–280 °C in an argon environment using a two-probe cell with graphite electrodes with an area of 0.25 cm^2, located at a distance of 0.4 cm from each other. Resistance values were obtained in the frequency range from 25 Hz to 1 MHz with an applied signal amplitude from 0.04 to 1 V.

Raman spectra were recorded using a Senterra confocal Raman microscope (Bruker, Germany). Raman spectra were measured in the range from room temperature to 340 °C with laser excitation (λ = 532 nm and power 20 mW), spectral measurement range of 50–1500 cm^{-1} with a resolution of 3–5 cm^{-1}, integration time for each scan was 20 s. To measure Raman spectra, the samples were sealed in Pyrex ampoules after air and moisture had been pumped out using a vacuum pump at a temperature of 100 °C.

To obtain true contours of the bands, the spectra of the original complex contours of the spectral bands were decomposed into individual components, the shape of which was approximated by curves of convolution of Gaussian and Lorentz functions. Fitting of the calculated curves and the original spectrum with minimization of the absolute error was carried out using the Levenberg-Marquardt method. The error between the calculated and real curves was 5–10 % depending on the signal-to-noise ratio of the original spectrum. All the procedures for processing Raman spectra were implemented using the OPUS 6.0 software package.

3. Results and discussion

3.1. The (1–x) $NaClO_4$ – x Al_2O_3 composite

3.1.1. Thermal analysis

DSC curves of the salt and the composites are shown in Figure 1.

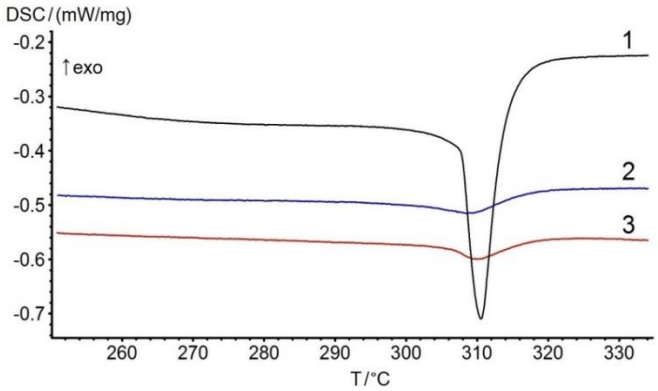

Figure 1 DSC curves of $NaClO_4$ (1), $0.7NaClO_4 – 0.3Al_2O_3$ (2) and $0.4NaClO_4 – 0.6Al_2O_3$ (3).

Table 1 – Phase transition enthalpy of sodium perchlorate in the $(1–x)\,NaClO_4 – x\,Al_2O_3$ composites (calculated with reference to the mass of $NaClO_4$).

Composition	ΔH, J/g
$NaClO_4$	12.5
$0.7NaClO_4 – 0.3Al_2O_3$	5.2
$0.4NaClO_4 – 0.6Al_2O_3$	4.7

While heating sodium perchlorate, a structural phase transition was recorded at 307.7 °C. As can be seen from Figure 1, the addition of aluminum oxide had a significant effect on the phase transition of $NaClO_4$.

The phase transition enthalpy of $NaClO_4$ was 12.5 J/g, in the $0.7NaClO_4 – 0.3Al_2O_3$ composite calculated with reference to the mass of pure salt – 5.2 J/g (Table 1). When the concentration of aluminum oxide was higher ($x = 0.6$), its effect on the structural phase transition enthalpy of $NaClO_4$ was even more significant. In addition to a decrease in the proportion of the salt component in the composite, a decrease in the enthalpy of the phase transition of sodium perchlorate may be associated with disordering of the structure of crystalline $NaClO_4$ (Figure 1) [18].

If we consider salt crystallinity as a ratio of the phase transition enthalpy of $NaClO_4$ in the composite to the phase transition enthalpy of pure $NaClO_4$, then the proportion of salt crystallinity in the composites with Al_2O_3 was less than 50 %. A decrease in the phase transition enthalpy might be associated with various factors, in particular, with amorphization of the salt, a violation of structural correspondence between the crystal lattices of the contacting phases, a decrease in crystallinity of the salt, disordering of the salt sublattice of the composite, and stabilization of the high-temperature phase of sodium perchlorate.

The effect of the oxide filler on phase transitions was previously noted for other salt-oxide composites [19].

Thus, it was found that in the $NaClO_4 – Al_2O_3$ composites, Al_2O_3 had a significant effect on enthalpy and temperature of the structural phase transition of sodium perchlorate. The addition of nanosized aluminum oxide resulted in a significant change in the microstructure of the $(1–x)\,NaClO_4 – x\,Al_2O_3$ composite [18].

3.1.2. Ionic conductivity

Figure 2 shows the temperature dependences of specific ionic conductivity for sodium perchlorate ($NaClO_4$) and composites based on it. The measurements showed that the values of specific ionic conductivity were well reproduced in heating-cooling cycles, and were also stable during a long-term exposure in vacuum under isothermal conditions. This fact suggests that conductivity of high-temperature phases is determined by the contribution of their own volume conductivity, but is not due to metastable defects, the contribution of surface conductivity or the effect of adsorbed moisture. Phase transitions and the values of specific ionic conductivity (Figure 2 and Table 2) at 320 °C for $NaClO_4$ – $2.49 \cdot 10^{-5}$ S/cm – are consistent with reported data [18, 21].

Linear sections on the temperature dependence of conductivity in the $0.7NaClO_4 – 0.3Al_2O_3$ and $0.4NaClO_4 – 0.6Al_2O_3$ systems (Figure 2) obtained after mechanical activation (MA) for 120 min show that conductivity is thermally activated. That is, with increasing temperature, the energy of thermal motion of $NaClO_4$ molecules increases, which leads to an increase in the rate of charge transfer and, consequently, to an increase in conductivity. Besides, in the $0.7NaClO_4 – 0.3Al_2O_3$ and $0.4NaClO_4 – 0.6Al_2O_3$ systems, there is no phase transition (Figure 2), a significant decrease in activation energy is observed, and the value of specific ionic conductivity increases by two orders of magnitude

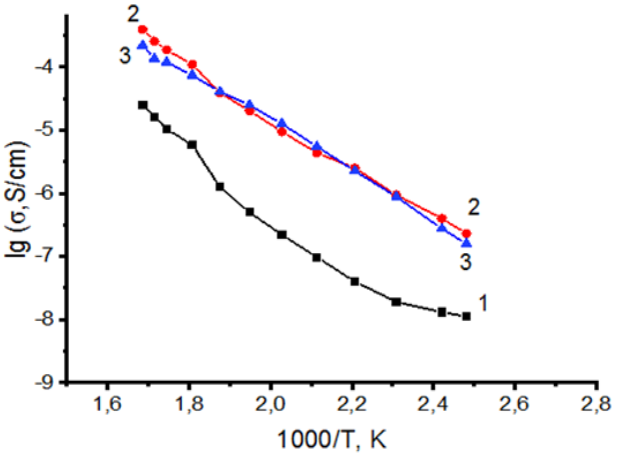

Figure 2 Temperature dependence of specific ionic conductivity of $NaClO_4$ (1) and the $0.7NaClO_4 – 0.3Al_2O_3$ (2) and $0.4NaClO_4 – 0.6Al_2O_3$ (3) composites.

Table 2 – Specific conductivity and activation energy of $NaClO_4$ and the $0.7NaClO_4 – 0.3Al_2O_3$ and $0.4NaClO_4 – 0.6Al_2O_3$ composites.

Composition	Temperature regions									
	I					*II*				
	σ_{AC}, S/cm (*T*, °C)	*T*, °C	E_a, J/mol	$\Delta(E_a)$, %	log*A*	σ_{AC}, S/cm (*T*, °C)	*T*, °C	E_a, J/mol	$\Delta(E_a)$, %	log*A*
$NaClO_4$	$5.83 \cdot 10^{-6}$ (280)	140–280	65.28	0.08	–0.16	$2.49 \cdot 10^{-5}$ (320)	290–320	98.15	0.09	1.39
$0.7NaClO_4 – 0.3Al_2O_3$	$5.95 \cdot 10^{-4}$ (320)	140–320	76.64	0.03	1.19	–	–	–	–	–
$0.4NaClO_4 – 0.6Al_2O_3$	$3.18 \cdot 10^{-4}$ (320)	140–320	74.11	0.03	0.97	–	–	–	–	–

compared to $NaClO_4$ [22, 7].

Absolute conductivity values and the parameters of Arrhenius dependences $\sigma \cdot T = A \cdot \exp\left(^{-E_a}/_{kT}\right)$ for the studied $NaClO_4$ salt and its composites are presented in Table 2.

Two linear temperature sections (140–280 °C and 290–320 °C) for $NaClO_4$ salt that obey the Arrhenius equation on the curve of electrical conductivity versus temperature may indicate the presence of two different mechanisms that determine the electrical conductivity of the substance in different temperature ranges [22, 18]. It should be noted that the values of activation energy and specific ionic conductivity for the $0.7NaClO_4 – 0.3Al_2O_3$ and $0.4NaClO4 – 0.6Al_2O_3$ systems decrease with increasing aluminum oxide filler content.

3.1.3. Vibrational spectroscopy

The free perchlorate ion ClO^{-4} (Td symmetry) is characterized by the following Raman active vibrations: $\nu_1(A)$ is a fully symmetric stretching vibration (963 cm^{-1}), $\nu_2(E)$ is a doubly degenerate vibration (455 cm^{-1}), $\nu_3(F_2)$ is a triply degenerate vibration (1110 cm^{-1}), $\nu_4(F_2)$ is a triply degenerate vibration (619 cm^{-1}). In the Raman spectra of $(1–x)\,NaClO_4 – x\,Al_2O_3$ (Figure 3), the $\nu_1(A)$, $\nu_2(E)$, $\nu_4(F_2)$ and $\nu_3(F_2)$ vibrations are active in the spectral region of 100 – 1500 cm^{-1} under study [23].

As one can see from the presented survey spectra, at aluminum oxide $x \geq 0.3$, the contours of almost all bands corresponding to the degenerate internal vibrations of the perchlorate anion in the composite spectra at room temperature acquire a complex structure. The contour of the $\nu_1(A)$ band of the $0.4NaClO_4 – 0.6Al_2O_3$ composite registered at room temperature is identical to the contour of the band registered at a temperature above the phase transition temperature of pure $NaClO_4$ [24]. Based on the above, it can be assumed that a part of sodium perchlorate salt is amorphized in the phase contact region. The results of spectroscopic measurements are in good agreement with the DSC (Figure 1) and conductivity data.

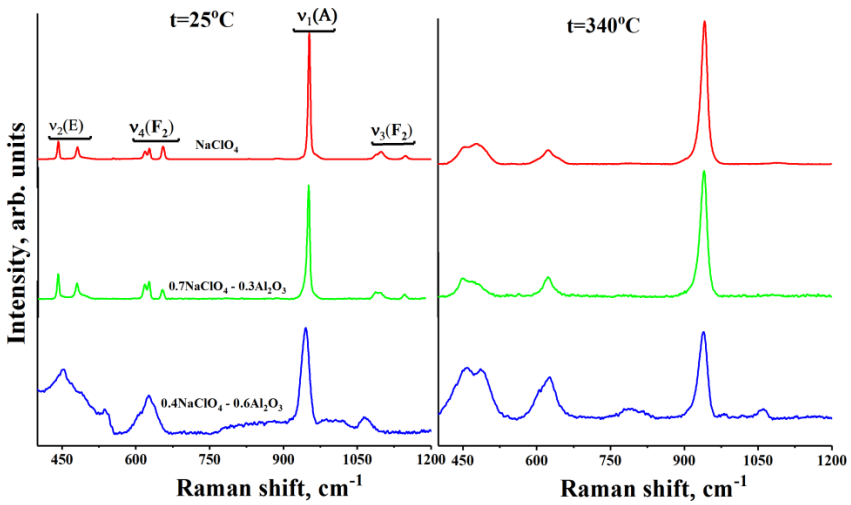

Figure 3 Raman spectra of $NaClO_4$ and the $0.7NaClO_4 – 0.3Al_2O_3$ and $0.4NaClO_4 – 0.6Al_2O_3$ composites registered at room temperature and $T = 340$ °C.

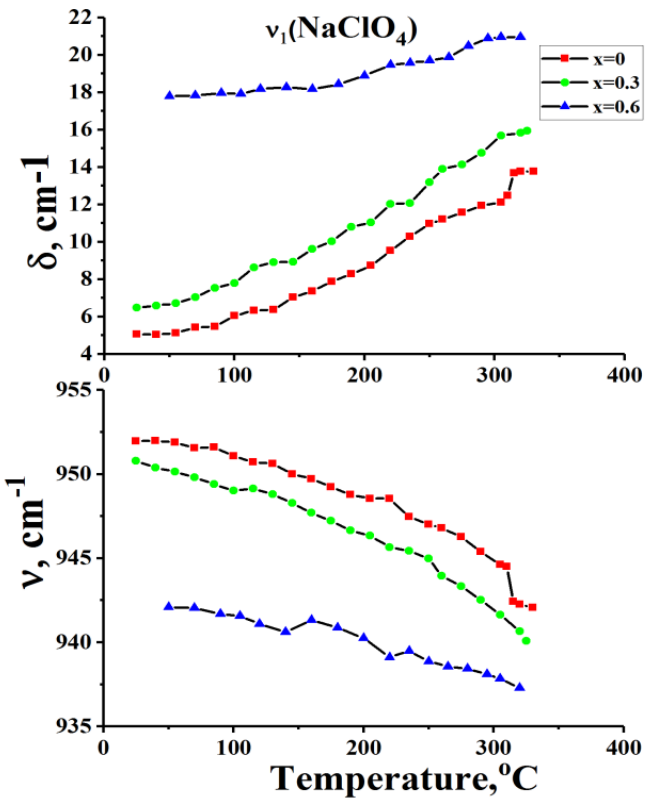

Figure 4 Temperature dependences of frequencies ν and half-widths δ of the $\nu_1 \sim 952$ cm^{-1} vibrations of the ClO^{4-} anion in the (1–x) $NaClO_4$ – x Al_2O_3 composites.

At high concentrations of aluminum oxide, the abrupt changes in spectral characteristics specific to a phase transition disappear [25]. We can assume that some disorder occurs in the salt subsystem under the influence of nanosized aluminum oxide (Figure 4).

3.2. The (1–x) $KClO_4$ – x γ–Al_2O_3 composite

3.2.1. Thermal analysis

DSC curves of the salt and the composites are shown in Figure 5.

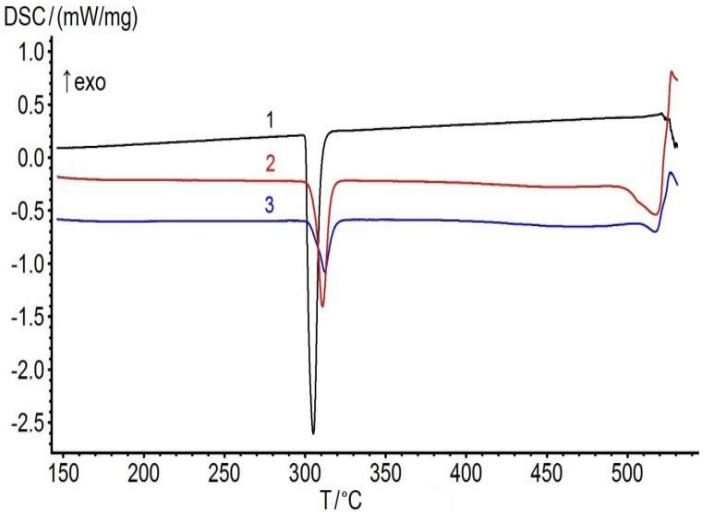

Figure 5 DSC curves of $KClO_4$ (1), 0.7$KClO_4$ – 0.3Al_2O_3 (2) and 0.4$KClO_4$ – 0.6Al_2O_3 (3).

As one can see from Figure 5, the decomposition temperature of $KClO_4$ in the composites decreases as compared to pure potassium perchlorate. At the same time, the temperature of the structural phase transition of potassium perchlorate at ~ 300 °C hardly shifts. The phase transition enthalpy of $KClO_4$ is 103 J/g, in the 0.7$KClO_4$ – 0.3Al_2O_3 composite calculated with reference to the mass of pure salt – 90 J/g, and in the composite containing 0.6 mole fraction of Al_2O_3 – 69 J/g. Thus, a higher content of aluminum oxide (x = 0.6) has a stronger effect on the structure of potassium perchlorate, which results in a more significant decrease in the phase transition enthalpy of $KClO_4$. The decrease in the enthalpy of the phase transition of potassium perchlorate can be related to the disordered structure of crystalline $KClO_4$ [19, 18].

3.2.2. Ionic conductivity

Figure 6 shows the temperature dependences of specific ionic conductivity for pure $KClO_4$ and composites based on it. It is known from that in $KClO_4$, a phase transition occurs at a temperature of 300 °C. In the dependences (Figure 6), phase transitions and the value of specific ionic conductivity for $KClO_4$ $2.98 \cdot 10^{-8}$ S/cm at 320 °C are consistent with reported data [7, 18].

In the 0.7$KClO_4$ – 0.3Al_2O_3 and 0.4$KClO_4$ – 0.6Al_2O_3 systems obtained after mechanical activation for 120 min, no phase transition is observed (Figure 6), the value of specific ionic conductivity for the 0.7$KClO_4$ – 0.3Al_2O_3 and 0.4$KClO_4$ – 0.6Al_2O_3 systems increases by several orders of magnitude as compared to the original electrolyte $KClO_4$.

Specific ionic conductivity of $KClO_4$ does not exceed $2.9 \cdot 10^{-8}$ S/cm at 320°C. With aluminum oxide additive, the maximum conductivity value is observed in the 0.4$KClO_4$ – 0.6Al_2O_3 composite and it reaches ~ $3.6 \cdot 10^{-5}$ S/cm at 320 °C.

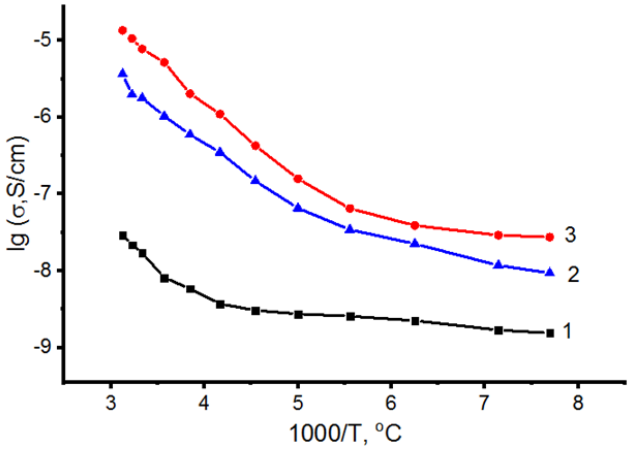

Figure 6 Temperature dependence of specific ionic conductivity of $KClO_4$ (1) and its composites 0.7$KClO_4$ – 0.3Al_2O_3 (2) and 0.4$KClO_4$ – 0.6Al_2O_3 (3).

Apparently, this may be due to the presence of amorphism at high temperatures in the composites under study after mechanical activation.

The presence of two linear sections (140–220 °C and 240–320 °C) on the curve of electrical conductivity versus temperature for $KClO_4$ may indicate a change in the mechanism of conductivity of the substance depending on temperature. For example, at low temperatures, the conductivity of $KClO_4$ can be determined by tunneling or charge transfer through defects in the crystal lattice, which can lead to a linear dependence of electrical conductivity on temperature. At higher temperatures, however, another mechanism, such as the thermal excitation of electrons, may become dominant, also leading to a linear dependence of electrical conductivity on temperature [19, 20].

Thus, the presence of two linear sections on the curve of electrical conductivity versus temperature for $KClO_4$ may indicate a complex mechanism of conductivity of this substance, which changes depending on temperature.

These values (Table 3) also confirm that the most optimal values of activation energy (E_a), ionic conductivity (σ) and pre-exponential factor (A) within the temperature range (140–320 °C) are observed for the $0.4KClO_4 – 0.6Al_2O_3$ system.

3.2.3. Vibrational spectroscopy

In the Raman spectra of $(1–x)\ KClO_4 + x\ Al_2O_3$, the ν_1 (A), ν_2 (E), ν_4 (F_2) and ν_3 (F_2) vibrations are active in the spectral region of 100–1500 cm^{-1} under study [23] (Figure 7).

Table 3 – Specific conductivity and activation energy of $KClO_4$ and the $0.7KClO_4 – 0.3Al_2O_3$, $0.4KClO_4 – 0.6Al_2O_3$ systems.

Composition	Temperature regions									
	I					*II*				
	σ_{AC}, S/cm (T, °C)	T, °C	E_a, J/mol	$\Delta(E_a)$, %	log$A$	σ_{AC}, S/cm (T, °C)	T, °C	E_a, J/mol	$\Delta(E_a)$, %	log$A$
$KClO_4$	$2.74 \cdot 10^{-9}$ (220)	140–220	12.59	0.09	1.97	$2.98 \cdot 10^{-8}$ (320)	240–320	65.62	0.07	0.58
$0.7KClO_4 – 0.3\ Al_2O_3$	$1.36 \cdot 10^{-6}$ (320)	140–320	70.97	0.05	0.83	–	–	–	–	–
$0.4KClO_4 – 0.6Al_2O_3$	$3.66 \cdot 10^{-5}$ (320)	140–320	62.77	0.04	0.47	–	–	–	–	–

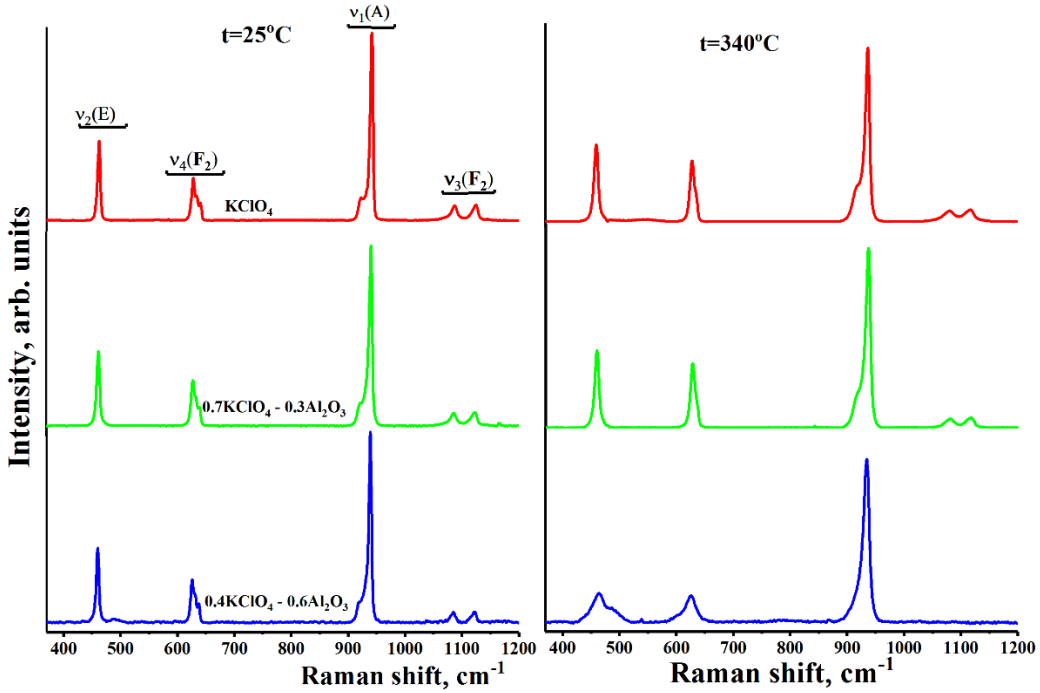

Figure 7 Raman spectra of pure $KClO_4$ and its composites $0.7KClO_4 – 0.3Al_2O_3$ and $0.4KClO_4 – 0.6Al_2O_3$ registered at room temperature and at T = 340 °C.

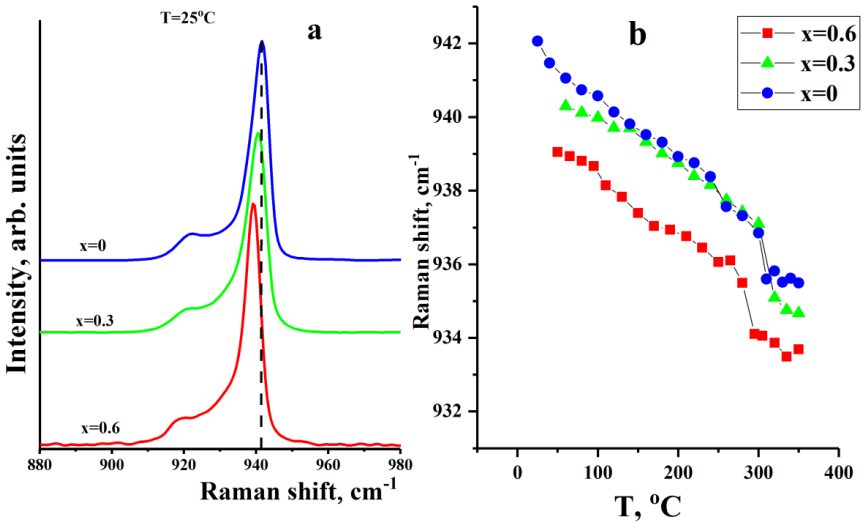

Figure 8 Raman spectra of the (1–*x*) $KClO_4$ – *x* Al_2O_3 composite registered at *T* = 25 °C in the region of fully symmetric vibration *и* (*A*) (a) and its temperature dependence (b).

Figure 8 presents Raman spectra of the (1–*x*) $KClO_4$ – *x* Al_2O_3 composite in the region of fully symmetric vibration *и* (*A*) of the perchlorate anion registered at room temperature (a) and its temperature dependence (b). The figure shows that at $x \leq 0.3$, aluminum oxide does not have a significant effect on the salt structure [26, 27].

At concentrations $x = 0.6$, one can observe a shift of *и* (*A*) to a low-frequency region, as well as a slight broadening of the band. Based on our previous works [28, 29], we can assume that some disorder occurs in the salt subsystem under the influence of nanosized aluminum oxide. This assumption is confirmed by an increase in ionic conductivity at $x = 0.6Al_2O_3$.

4. Conclusions

A decrease in the enthalpy of phase transitions of sodium and potassium perchlorate was revealed by DSC analysis. Based on electrochemical impedance spectroscopy data, it was established that for the $0.4NaClO_4 – 0.6Al_2O_3$ system subjected to mechanical activation, the value of specific ionic conductivity increased by two orders of magnitude as compared to that of pure $NaClO_4$ and was equal to $3.18 \cdot 10^{-4}$ S/cm at $T = 320$ °C. For the $0.4KClO_4 – 0.6Al_2O_3$ system, the value of specific ionic conductivity increased by three orders of magnitude compared to the initial salt and was equal to $3.66 \cdot 10^{-5}$ S/cm at $T = 320$ °C. It was also found that long-term (120 minutes) mechanical activation of the composite was the most effective for the synthesis of the composites based on $NaClO_4$ and $KClO_4$ salts. Conductivity growth at doping (introduction of the oxide additive Al_2O_3) of sodium and potassium perchlorates is connected with the specific adsorption of cations on the surface of the nanocrystalline oxide, leading to the formation of excessive defects in the near-surface region of the ionic salt crystal. It is possible that the excess point defects are current carriers. It should be noted that the absence of conductivity jumps on the Arrhenius dependences for the composites based on $NaClO_4$ and $KClO_4$ indicates the possibility of at least partial amorphization of the salt in the contact region of the phases [30].

Supplementary materials

No supplementary materials are available.

Funding

This research had no external funding.

Acknowledgments

This study was carried out using the instruments of the Analytical Center of Collective Use of the Dagestan Federal Research Center of the Russian Academy of Sciences.

Author contributions

Zaur Kubataev: Conceptualization; Project administration; Writing – Original draft.
Malik Gafurov: Conceptualization.
Kamil Rabadanov: Methodology.
Magomed Akhmedov: Visualization.
Akhmed Amirov: Methodology.

Conflict of interest

The authors declare no conflict of interest.

Additional information

https://www.researchgate.net/profile/Zaur-Kubataev.

References

1. Liang CC, Conduction Characteristics of the Lithium Iodide-Aluminum Oxide Solid Electrolytes, J. Electrochem. Soc., **120** (1973) 1289. https://doi.org/10.1149/1.2403248

2. Ulihin AS, Uvarov NF, Mateyshina YuG, Brezhneva LI, et al., Composite solid electrolytes $LiClO_4$-Al_2O_3, Solid State Ionics, **177(26–32)** (2006) 2787–2790. https://doi.org/10.1016/j.ssi.2006.03.018

3. Zhang Z, Wang X, Li X, Zhao J, et al., Review on composite solid electrolytes for solid-state lithium-ion batteries, Materials Today Sustainability, **21** (2023) 100316. https://doi.org/10.1016/j.mtsust.2023.100316

4. Ulihin AS, Uvarov NF, Electrochemical properties of composition solid electrolytes $LiClO_4$-MgO, Russ. J. Electrochem., **45** (2009) 707–710. https://doi.org/10.1134/S1023193509060135

5. Zou Z, Li Y, Lu Z, Wang D, et al., Mobile Ions in Composite Solids, Chem. Rev., **120(9)** (2020) 4169–4221. https://doi.org/10.1021/acs.chemrev.9b00760

6. Mateyshina Y, Slobodyuk A, Kavun V, Uvarov N, Conductivity and NMR study of composite solid electrolytes $CsNO_2$-A (A = SiO_2, Al_2O_3, MgO), Solid State Ionics, **324** (2018) 196–201. https://doi.org/10.1016/j.ssi.2018.04.026

7. Uvarov NF, Composite solid electrolytes: recent advances and design strategies, J. Solid State Electrochem., **15(2)** (2011) 367–389. https://doi.org/10.1007/s10008-008-0739-4

8. Xu Z, Zheng L, Chen B, Zhang T, et al., Overview of research on composite electrolytes for solid-state batteries, Energy Storage Science and Technology, **10(6)** (2021) 2117–2126. https://doi.org/10.19799/j.cnki.2095-4239.2021.0178

9. Uvarov NF, Ulihin AS, Mateyshina YuG, Nanocomposite alkali-ion solid electrolytes, Advanced Nanomaterials for Catalysis and Energy, (2022) 393–434. https://doi.org/10.1016/B978-0-12-814807-5.00011-5

10. Reddy YG, Sekhar MCh, Chary AS, et al., Ion transport studies on $Pb(NO_3)_2$:Al_2O_3 composite solid electrolytes: Effect of dispersoid particle size, IOP Conf. Ser.: Mater. Sci. Eng., **310** (2018) 012160. https://doi.org/10.1088/1757-899X/310/1/012160

11. Aziam H, Larhrib B, Hakim Ch, Sabi N, et al., Solid-state electrolytes for beyond lithium-ion batteries: A review, Renewable and Sustainable Energy Reviews, **167** (2022) 112694. https://doi.org/10.1016/j.rser.2022.112694

12. Uvarov NF, Ulihin AS, Slobodyuk AB, Kavun VY, et al., Nanocomposite Solid Electrolytes Based on Lithium Perchlorate, ECS Transactions, **11(31)** (2008) 9–17. https://doi.org/10.1149/1.2953501

13. Leonardi M, Villacampa M, Menéndez JC, Multicomponent mechanochemical synthesis, Chemical Science, **9** (2018) 2042–2064. https://doi.org/10.1039/c7sc05370c

14. Lee W, Lyon CK, Seo J-H, Lopez-Hallman R, et al., Ceramic–salt composite electrolytes from cold sintering, Advanced Functional Materials, **29(20)** (2019) 1807872. https://doi.org/10.1002/adfm.201807872

15. Gupta SK, Mao Y, A review on molten salt synthesis of metal oxide nanomaterials: Status, opportunity, and challenge, Progress in Materials Science, **117** (2021) 100734. https://doi.org/10.1016/j.pmatsci.2020.100734

16. Liu X, Fechler N, Antonietti M, Salt melt synthesis of ceramics, semiconductors and carbon nanostructures, Chemical Society Reviews, **42** (2013) 8237–8265. https://doi.org/10.1039/c3cs60159e

17. Gonzalo-Juan I, Riedel R, Ceramic synthesis from condensed phases, ChemTexts, **2** (2016) 6. https://doi.org/10.1007/s40828-016-0024-6

18. Ulikhin AS. Transport properties of alkali metal perchlorates and composite solid electrolytes based on them [dissertation]. Novosibirsk (Russia): Russian Academy of Sciences, Siberian Branch, Institute of Solid State Chemistry and Mechanochemistry; 2009. 125 p.

19. Amirov AM, Suleymanov SI, Gafurov MM, et al., Study of the MNO_3–Al_2O_3 nanocomposites by differential scanning calorimetry, J Therm. Anal. Calorim., **147** (2022) 9283–9290. https://doi.org/10.1007/s10973-022-11256-0

20. Akhmedov MA, Gafurov MM, Rabadanov KSh, et al., Effect of mechanoactivation on the structure and electrical conductivity in the KNO_3-Al_2O_3 system, Russian Journal of Electrochemistry, **59(8)** (2023) 465–473. In press. https://doi.org/10.31857/S0424857023080030

21. Chen X, Kuroda DG, Ionic conduction mechanism in high concentration lithium ion electrolytes, Chem. Commun., **59** (2023) 1849–1852. https://doi.org/10.1039/D2CC05645C

22. Ulihin AS, Uvarov NF, Rabadanov KSh, Gafurov MM, et al., Thermal, structural and transport properties of composite solid electrolytes (1-x)$(C_4H_9)_4NBF_4$–xAl_2O_3, Solid State Ionics, **378** (2022) 115889. https://doi.org/10.1016/j.ssi.2022.115889

23. Snezhkov VI. Nonlinear inter-ion multiparticle interactions in molten and solid electrolytes [dissertation]. Rostov-on-Don (Russia): North–Caucasian Scientific Center of Higher Education, Rostov-on-Don State Academy of Construction; 1994. 302 p.

24. Gafurov MM, Rabadanov KSh, High-temperature vibrational spectroscopy of molten electrolytes, Appl. Spectrosc. Rev., **58(7)** (2022) 489–508. https://doi.org/10.1080/05704928.2022.2048305

25. Kalampounias AG, Kirillov SA, Steffen W, Yannopoulos SN, Raman spectra and microscopic dynamics of bulk and confined salol, J. Mol. Struct., **651–653** (2003) 475–483. https://doi.org/10.1016/S0022-2860(03)00128-5

26. Gafurov MM, Rabadanov KSh, Kubataev ZYu, et al, Vibrational relaxation of perchlorate ion in the (1–x)$LiClO_4$ + xAl_2O_3 nanocomposites, Bulletin of Dagestan State University. Series 1. Natural Sciences, **34(3)** (2019) 102–108. https://doi.org/10.21779/2542-0321-2019-34-3-102-108

27. Gafurov MM, Rabadanov KS, Ataev MB, Amirov AM, et al., Research of the structure and dynamic interactions of particles in the $Li_{0.42}K_{0.58}NO_3$–R (R = α-Al_2O_3, γ-Al_2O_3, SiO_2) and ($LiNO_3$–$LiClO_4$) – γ-Al_2O_3 composites in various temperature conditions and phase states, Spectrochimica Acta Part A: Molecular and Biomolecular Spectroscopy, **257** (2021) 119765. https://doi.org/10.1016/j.saa.2021.119765

28. Uvarov N, Ulihin A, Ponomareva V, Kovalenko K, et al., Effect of Pore Filling on Properties of Nanocomposites $LiClO_4$–MIL–101(Cr) with High Ionic Conductivity, Nanomaterials, **12(19)** (2022) 3263. https://doi.org/10.3390/nano12193263

29. Abramczyk H, Paradowska-Moszkowska K, The correlation between the phase transitions and vibrational properties by Raman spectroscopy: Liquid solid β and solid β-solid α acetonitrile transitions, Chem. Phys., **265(2)** (2001) 177–191. https://doi.org/10.1016/S0301-0104(01)00271-3

30. Hosaka T, Kubota K, Kojima H, et al., Highly concentrated electrolyte solutions for 4 V class potassium-ion batteries, Chemical Communications, **54(60)** (2018) 8387–8390. https://doi.org/10.1039/c8cc04433c